arXiv:1401.4290v2 [physics.optics] 1 Aug 2014

Supplementary Material

Mattia Lupetti[a], Julia Hengster[b], Thorsten Uphues[b], and Armin Scrinzi[a*]
[a] *Physics Department, Ludwig Maximilians Universität, D-80333 Munich, Germany and*
[b] *Center for Free-Electron Laser Science, Universität Hamburg, D-22761 Hamburg, Germany*

PARAMETERIZATION OF THE PLASMON

The variance of the photoscopic spectrogram according to our theory is given by:

$$S(\tau) = \Delta p^2 + \frac{1}{\pi}\int_{-\infty}^{\infty} dx_i\, g_{\mathrm{x}}(x_i)\, \mathbf{a}_y^2(x_i,\tau). \qquad (1)$$

In order to compute the spatial integral in Eq. (1), we consider a case where the bright and dark modes can both be excited at frequencies ω_b and ω_d, respectively. "Bright" and "dark" refer to the coupling properties of the modes: the bright mode couples efficiently with incident radiation, the dark poorly. The two frequencies are well separated. Each mode consists of two counter-propagating plasmons. In addition, we admit a term describing the ringing of localized modes excited in the focus of the NIR pulse (see, e.g., [1]). The contributions in each mode $m = b, d$ are

$$P_m^{(\pm)} = e^{i\varphi_{\pm m}} e^{-\frac{\varphi_{\pm m}^2}{2\omega_m^2 T_m^2}} \qquad (2)$$

with the phase of the propagating plasmon

$$\varphi_{\pm m} = \pm k_m x - \omega(t - t_m) \qquad (3)$$

and

$$P_m^{(0)} = \cos(\omega_m(t-t_m))\, e^{-x^2/2w_{\mathrm{nir}}^2}, \qquad (4)$$

for the localized excitation.

Buildup and decay are assumed to obey a simple rate equation where a Gaussian-shaped buildup of width σ is depleted by decay at a constant rate τ:

$$\dot f(t) = e^{-\frac{t^2}{2\sigma^2}} - \frac{1}{2\tau} f(t). \qquad (5)$$

The resulting time-distribution is

$$\begin{aligned} f(t,\sigma,\tau) &= \int_0^t e^{-\frac{t'^2}{2\sigma^2}} e^{-\frac{t-t'}{2\tau}}\, dt' \\ &= e^{\frac{\sigma^2-4\tau t}{8\tau^2}} \left[1 - \mathrm{erf}\left(\frac{\sigma^2 - 2\tau t}{2\sqrt{2}\tau\sigma}\right)\right]. \end{aligned} \qquad (6)$$

With this, the complete field is parametrized by

$$\begin{aligned} \mathsf{a}_y(x,t) = \sum_{m=b,d} & f(t-t_m,\sigma_m,\tau_m) \\ & \times \left\{ \mathrm{a}_m \left[P_m^{(+)} - P_m^{(-)}\right] + \mathrm{c}_m P_m^{(0)} \right\}. \end{aligned} \qquad (7)$$

In practice, we find that the bright mode decays so fast that its propagation can be neglected in the spectrogram variance and we set $\mathrm{a}_b \equiv 0$.

We define the buildup time of each mode $\xi_m = \sigma_m\sqrt{\ln(2)}$ as the half-width half-maximum of the Gaussian function in Eq. (6), which allows for a direct comparison with the NIR pulse FWHM duration.

The dark mode plasmon duration T has a measurable effect only during generation, when counter-propagating SPPs have not separated yet and form a standing wave. As this process is superposed by the bright mode, it cannot be reliably retrieved from the fit. However, T is only weakly correlated with the dynamical parameters ξ_m, τ_m and ω_m. Table I shows the dynamical parameters for variations of T over $[10, 20]$ fs (FWHM).

TABLE I. Buildup-, life-time, and frequency of the bright and dark modes as obtained by fitting Eq. (1) with the parameterization (7), for a range of plasmon durations T_m. Times in fs, frequencies in eV, $T_{\mathrm{FWHM}} = 2\sqrt{\ln 2}T$.

T	6	7	8	9	10	11	12	Var
T_{FWHM}	9.99	11.66	13.32	14.99	16.65	18.32	19.98	
ξ_b	1.933	1.964	1.987	2.004	2.016	2.025	2.031	5 %
τ_b	3.285	3.137	3.031	2.964	2.924	2.903	2.896	13 %
ξ_d	5.941	5.649	5.430	5.286	5.202	5.160	5.149	15 %
τ_d	34.18	34.41	34.57	34.63	34.62	34.57	34.47	< 1 %
ω_b	1.613	1.615	1.616	1.617	1.617	1.616	1.615	< 1 %
ω_d	1.645	1.645	1.645	1.645	1.645	1.645	1.645	< 1 %

[1] F.C. Garcia-Vidal *et al.*, J. Lightwave Technology **17**, 2191 (1999).

arXiv:1401.4290v2 [physics.optics] 1 Aug 2014

Attosecond Photoscopy of Plasmonic Excitations

Mattia Lupetti[a], Julia Hengster[b], Thorsten Uphues[b], and Armin Scrinzi[a]*
[a] *Physics Department, Ludwig Maximilians Universität, D-80333 Munich, Germany and*
[b] *Center for Free-Electron Laser Science, Universität Hamburg, D-22761 Hamburg, Germany*
(Dated: August 4, 2014)

We propose an experimental arrangement to image, with attosecond resolution, transient surface plasmonic excitations. The required modifications to state-of-the-art setups used for attosecond streaking experiments from solid surfaces only involve available technology. Buildup and life times of surface plasmon polaritons can be extracted and local modulations of the exciting optical pulse can be diagnosed *in situ*.

Surface plasmons are collective excitations of electrons that propagate along a metal-dielectric interface. Recently, plasmonics has gathered interest for the development of ultra-fast all-optical circuitry [1], since it can combine the high operational speed of photonics (PHz scale) with the miniaturization provided by electronics (nm scale). For this purpose, it is important to understand the buildup dynamics and lifetime of the collective electronic excitation. Although the plasmon lifetime can be inferred from the plasmonic resonance width (of the transmission spectrum, see for instance [2]), plasmon buildup is a process that cannot be addressed in terms of frequency analysis.

In the present work, we propose an experimental setup to image the transient dynamics of a plasmonic mode, which can be realized as a modification of the so-called "attosecond streak camera" [3], which has already been successfully applied to solid surfaces. The attosecond streak camera is a two-color pump-probe scheme, where a weak XUV attosecond pulse ionizes electrons from the solid, and a collinear, few-cycle ($\sim 5\,fs$ FWHM) NIR pulse serves as the probe, which accelerates the XUV photo-electrons after their escape from the solid. With this technique it was possible to resolve solid-state physics phenomena with resolution of a few attoseconds ($1\,\mathrm{as} = 10^{-18}$ s) [4].

We benchmark our setup concept against the buildup of Surface Plasmon Polaritons (SPPs) excited by a NIR pulse on a grating surface. A time-delayed XUV pulse probes the SPPs during their evolution by detecting the effect of their field on XUV photoemission. In principle, pump and probe beams can be spatially separated, allowing to probe different surface regions. Thus, differently from atomic and surface streaking employed so far, the setup provides spatio-temporal information. To distinguish it from standard attosecond streaking experiments, we name our setup "attosecond photoscopy".

A well established method for producing isolated attosecond pulses is the generation of high harmonic radiation (HHG) in noble gases [4–7]. An intense few cycle NIR laser pulse is focused into a noble gas target and generates high harmonics of the fundamental radiation. The XUV radiation co-propagates with the driving laser pulse. Both pulses are focused onto a sample with a delayable two part mirror composed of an XUV multilayer mirror in the inner part and a broadband NIR mirror in the outer part. The multilayer mirror is designed as a high pass filter for the harmonics, which results in an isolated attosecond pulse. The pulse can be timed relative to the NIR with a precision of $\lesssim 10\,as$.

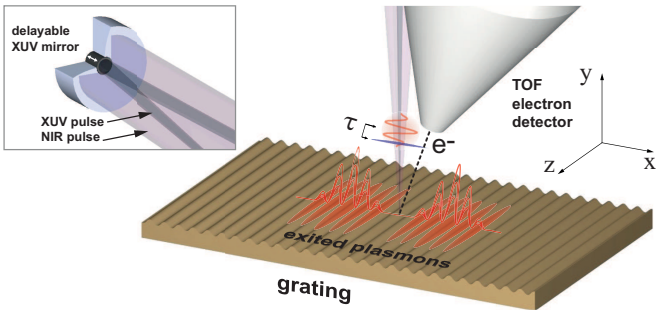

FIG. 1. Experimental setup of an attosecond photoscopy experiment. The XUV attosecond pulse liberates electrons in presence of the plasmonic field, which is excited by a short NIR pulse. Control of NIR-XUV time delay τ allows observation of the plasmon transient dynamics.

Figure 1 illustrates the setup discussed here. The NIR and XUV beams propagate in y-direction, at normal incidence onto the plane of the grating. Polarizations are in x-direction, perpendicular to the grooves. Using this arrangement, two counter-propagating plasmons are excited in the focus of the NIR pulse on the grating structure. A band gap at the zero crossing separates two plasmon branches [8]. An optical pulse at normal incidence usually couples to only one of the branches, called the bright mode, but at tight focussing with about 5° angular dispersion also the second, "dark" mode is excited.

XUV photo-electrons are measured at perpendicular direction to the surface. As in [4], the final electron momenta are recorded as a function of the delay between the NIR and XUV beams. The electron *spectrogram* retrieved is a convolution of photoemission with acceleration in the plasmonic field at the location and time of the initial electron release.

Depending on the time delay between the NIR pulse and the probing attosecond pulse, the XUV generated photoelectrons experience a different plasmonic field am-

plitude and phase, leading to a modulation of the kinetic energy distribution by the emerging plasmonic field.

The energy gap between dark and bright modes manifests itself in the spectrogram as a "transition" from the bright ω_b to the dark ω_d mode frequencies, which is measurable in our setup because of the attosecond resolution.

Below we analyze the photoscopic spectrogram using a basic analytical model as well as numerical solutions of the SPP propagation together with a Monte Carlo simulation of the electron streaking process. We will demonstrate that from the spectrograms one can recover the plasmonic field at the surface. The detailed analysis and interpretation will be discussed in the following.

Standard streaking experiments are based on electron sources that can be considered point-like with respect to the laser wavelength, such as atoms or molecules. For this reason the dipole approximation can be used: $\mathbf{A}(\mathbf{r},t) \simeq \mathbf{A}(t)$. After emission, the electron canonical momentum is conserved: $\mathbf{P}(t) = \mathbf{P}_i$, which translates into $\mathbf{p}(t) + \frac{e}{c}\mathbf{A}(t) = \mathbf{p}_i + \frac{e}{c}\mathbf{A}(t_i)$, where e denotes the electron charge and $|\mathbf{p}_i| = \sqrt{2m(E_{xuv} - W_f)}$ is the initial momentum of the electron released at time t_i from a material with work function W_f. Assuming that $A(t \to \infty) = 0$, the final momentum recorded by the spectrometer is

$$\mathbf{p}_f = \mathbf{p}_i + \mathbf{a}(t_i), \tag{1}$$

where we defined $\mathbf{a} := \frac{e}{c}\mathbf{A}$.

The spectral width of the XUV attosecond pulse is reflected in a momentum-broadening of the initial electron distribution $n_e = n_e(\mathbf{p}_i, t_i)$. For simplicity we assume Gaussian distributions centered around momentum $\mathbf{p}_0$ and time t_0, respectively, where t_0 denotes the time of peak XUV intensity on target. With Eq. (1) for the initial electron momentum, the time-integrated final momentum is

$$\sigma(\mathbf{p}_f) = \int_{-\infty}^{\infty} dt_i \, n_e(\mathbf{p}_f - \mathbf{a}(t_i), t_i). \tag{2}$$

The spectrogram for a series of delays τ becomes

$$\sigma(\mathbf{p}_f, \tau) = \int_{-\infty}^{\infty} dt_i \, n_e(\mathbf{p}_f - \mathbf{a}(t_i), t_i - \tau). \tag{3}$$

From this, the NIR pulse can be reconstructed by analyzing the average momentum of the streaking spectrogram

When applying the method to plasmonic excitations we have to consider that the SPP, acting as the streaking field, is spatially inhomogeneous and propagates on a surface. Previous work on streaking on nanoparticles [9] clearly shows that spatial inhomogeneity of the streaking field leads to a smearing of the streaking trace obtained in a traditional setup. Thus, we need to include the position dependence into our initial electron distribution: $n_e(\mathbf{p}_i, t_i) \to n_e(\mathbf{r}_i, \mathbf{p}_i, t_i)$. The final momentum of the electrons accelerated in the plasmon field is then

$$\mathbf{p}_f = \mathbf{p}_i - e \int_{-\infty}^{\infty} \mathbf{E}(\mathbf{r}(t'), t') \, dt'. \tag{4}$$

For a typical XUV photon energy of 80 eV, the average initial speed of a photoelectron is $v_i = 5$ nm/fs. If the NIR pulse is 4 fs short, it will give rise to a plasmonic field of a duration of few tens of femtoseconds. During this time, the electrons move by $\lesssim 100$ nm. The additional drift imparted by the plasmonic field is small compared to the initial velocity. As the plasmon evanescent field extends to about NIR wavelength (800 nm) beyond the surface, we can write $\mathbf{r}(t') \simeq \mathbf{r}_i$ in Eq. (4). With this approximation, one obtains a position corrected analog of Eq.(1):

$$\mathbf{p}_f = \mathbf{p}_i - \mathbf{a}(\mathbf{r}_i, t_i) \tag{5}$$

Since the photoelectron detector does not resolve the emission positions $\mathbf{r}_i$, the photoscopic spectrogram is the integral over time *and the area covered by the XUV pulse*

$$\sigma(\mathbf{p}_f, \tau) = \int_{\mathbb{R}^3} d^3 r_i \int_{-\infty}^{\infty} dt_i \, n_e(\mathbf{r}_i, \mathbf{p}_f - \mathbf{a}(\mathbf{r}_i, t_i), t_i - \tau). \tag{6}$$

The space-averaged momentum is independent of the time-delay, as the integral of a propagating pulse is negligible (exactly zero in free space). Thus for extracting time information from the photoscopic spectrogram, we use the delay-dependent momentum variance

$$S(\tau) = \frac{\int d\mathbf{p}_f \, |\mathbf{p}_f|^2 \, \sigma(\mathbf{p}_f, \tau)}{\int d\mathbf{p}_f \, \sigma(\mathbf{p}_f, \tau)} - |\langle \mathbf{p}_f \rangle|^2. \tag{7}$$

As the XUV pulse duration is short compared to the NIR period, we treat photoemission as instantaneous. The distribution of the photoelectron yield along the surface is proportional to the XUV intensity profile. Furthermore, we neglect any transport effect in the solid and consider only the photoelectrons coming from the first few layers of material, as reported in [10]. With these conditions one finds

$$n_e(\mathbf{r}_i, \mathbf{p}_i, t_i - \tau) \simeq g_{\mathrm{x}}(x_i) n_e(\mathbf{p}_i) \delta(y_i - y_s) \delta(t_i - \tau - t_0),$$

where y_s is the grating vertical position (we neglect any groove depth effect) and g_{x} is a Gaussian function of width w_{x}, i.e. the XUV attosecond pulse focal spot.

As for the angular dependence of the photoemission we first restrict our discussion to the two extreme cases of 1) unidirectional emission with all initial momenta orthogonal to the grating plane, and 2) isotropic emission. For either distribution, the reconstructed times closely reproduce the actual dynamics. In reality, the XUV photoelectron distribution will be between these extreme cases and should be determined in a measurement without NIR field.

Unidirectional initial distributions can be written as $n_e(\mathbf{p}_i) = n_e(p_i \, \hat{\mathbf{n}}_s)$, where $p_i = |\mathbf{p}_i|$ and $\hat{\mathbf{n}}_s$ is the direction orthogonal to the grating plane. Eq. (6) now becomes

$$\sigma(p_f, \tau) = \int_{-\infty}^{\infty} dx_i \, g_{\mathrm{x}}(x_i) n_e \left(p_f - \hat{\mathbf{n}}_s \cdot \mathbf{a}(x_i, t_0 - \tau)\right),$$

where $\hat{\mathbf{n}}_s$ denotes the surface normal. Near the surface, in the region that is probed by the electrons, the plasmonic field is predominantly perpendicular to the surface. Therefore, we can approximate $\hat{\mathbf{n}}_s \cdot \mathbf{a} = \mathsf{a}_y \simeq \mathsf{a}_{\rm spp}$. Computing the variance Eq. (7) for a Gaussian distribution of the initial electron momenta, we obtain

$$S(\tau) = \Delta p^2 + \int_{-\infty}^{\infty} dx_i \, g_{\rm x}(x_i) \mathsf{a}^2_{\rm spp}(x_i, t_0 - \tau). \quad (8)$$

For isotropic XUV photo-electron emission, the initial distribution can be written as: $n_e(\mathbf{p}_i) = \frac{1}{\pi} n_e(p_i) = \frac{1}{\pi} n_e(|\mathbf{p}_f - \mathbf{a}|)$, where we employed $p_i = |\mathbf{p}_i|$. We use $|\mathbf{a}| \ll |\mathbf{p}_f|$ to approximate $|\mathbf{p}_f - \mathbf{a}| \simeq p_f - \mathbf{a} \cdot \hat{\theta}$, where θ is the angle between the final momentum and the surface normal. The spectrogram then reads

$$\sigma(p_f, \tau) = \frac{1}{\pi} \int_{-\infty}^{\infty} dx_i \, g_{\rm x}(x_i) \, n_e(p_f - \mathbf{a} \cdot \hat{\theta}). \quad (9)$$

A straightforward calculation for the angular integrations leads to the expression of the variance

$$S(\tau) = \Delta p^2 + \frac{1}{\pi} \int_{-\infty}^{\infty} dx_i \, g_{\rm x}(x_i) |\mathbf{a}(x_i, \tau)|^2. \quad (10)$$

In either case, by Eqs. (8) and (10), measuring the variance of the photo-emission spectrogram provides direct access to the space-averaged vector potential $\mathbf{a}^2$ at the surface in the direction of photo-detection. The surface vector potential $|\mathbf{a}|^2 = \mathsf{a}_x^2 + \mathsf{a}_{\rm spp}^2$ also includes a_x, the NIR field at the grating surface. Modifications of the surface field compared to the incident beam can be measured *in situ* (see below).

Simulations of the plasmonic field were performed with the finite-difference time-domain (FDTD) method [11], using a freely available software package [12]. Material properties were included through the appropriate model of gold dielectric function [13]. We assume a Gaussian 4 fs FWHM pulse at a central wave length of 800 nm. The grating parameters are optimized for maximal absorption from the NIR pulse, assuming a gold surface. Beam waists of NIR and XUV were 5 and 10 μm, respectively.

The XUV photoemission process is approximated as a sudden ejection of electrons from the surface boundary, with the appropriate unidirectional and isotropic initial momentum distribution, respectively. The electron trajectories and final momenta are computed by solving the Lorentz equation for each photoelectron in the previously simulated electromagnetic field.

The spectrogram variance obtained by Monte Carlo simulation is compared in Fig. 2 with the space integral of the squared vector potential along y from the FDTD simulation. We assume isotropic initial momentum distribution and a TOF detector of 5° acceptance centered around the perpendicular direction.

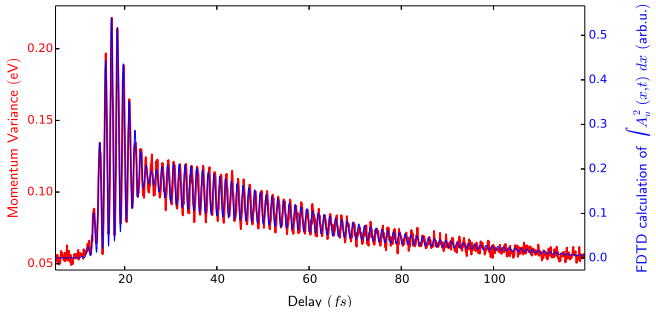

FIG. 2. Comparison between variance of photoscopic spectrogram in the "filtered isotropic" case (red) and $\int |\mathsf{a}_y|^2 dx$ computed in the FDTD (blue). The offset of the filtered isotropic case is due to the XUV pulse energy width.

Note that the variance directly images the integral of the surface plasmonic field squared without further assumptions or input from theory. The agreement is robust w.r.t. to the angular distribution of photo-electron momenta: one obtains analogous results for unidirectional emission.

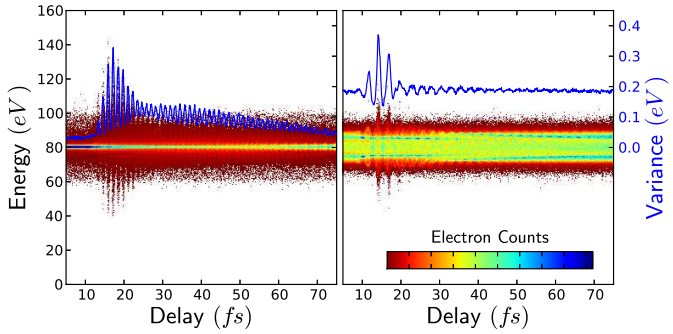

FIG. 3. Photoscopic spectrograms at perpendicular (left) and grazing (right) electron emission. The measurements retrieve plasmonic and NIR field, respectively. Solid lines are the momentum variances.

The detailed image of the fields provides for an *in situ* diagnosis both, of the plasmon field and exciting NIR source, including possible distortions due to the NIR reflection on the grating. In Figure 3 spectrograms observed in the perpendicular and grazing direction are shown, which reflect the two contributions.

From the plasmonic (perpendicular) component, we extract buildup and life-times, as well as contributions of the bright and dark modes to the spectrograms. We parametrize the field as follows: we assume plasmonic fields with a Gaussian envelope $\mathsf{a}_{\rm spp} = \exp[i\varphi] \exp[-\varphi^2/2\omega_{\rm spp}^2 T^2]$, with $\varphi = k_{\rm spp} x - \omega_{\rm spp} t$. There are two counter-propagating SPP wave-packets, each containing a bright ω_b and and a dark ω_d frequency. These terms are multiplied by a "buildup" and "decay" function $f(t) = \exp(-t/2\tau_m) \times (1 - \mathrm{erf}((\sigma_m^2 - 2\tau_m t)/(2\sqrt{2}\sigma_m \tau_m)))$, which is the convolution of a Gaussian excitation profile with exponential decay. Source du-

TABLE I. Carrier frequency ω_m, buildup time ξ_m and lifetime τ_m resulting from fits of the theoretical model to the numerically simulated data. The cases isotropic emission with perpendicular detection ("filtered"), unidirectional emission, as well as values extracted directly from the FDTD calculation are shown. (Times in fs. Frequencies in eV)

	Filtered Isotropic	Unidirectional	FDTD
ξ_b	2.07	2.06	2.01
τ_b	3.0	3.1	2.96
ξ_d	6.6	6.2	5.3
τ_d	32.5	33.3	34.6
ω_b	1.61	1.62	1.62
ω_d	1.65	1.65	1.65

ration and plasmon mode decay rate are denoted by σ_m and τ_m, respectively, for $m = b, d$. When $f(t)$ multiplies the plasmonic term, the respective τ_m parametrizes the lifetime, while the Gaussian half-width half-maximum in intensity $\xi_m = \sigma_m\sqrt{\ln 2}$ parametrizes the buildup time.

The remaining fit parameters are the amplitudes of the respective plasmon modes. The explicit form of the parametrization is given in the supplementary materials. The relevant free parameters in this model are the excitation buildup times ξ_b, ξ_d, the plasmon decay times τ_b, τ_d and the plasmon frequencies ω_b, ω_d for the bright and dark modes, respectively.

Fitting to the simulated variance, we find plasmon frequencies are $\hbar\omega_b = 1.65$ eV and $\hbar\omega_d = 1.62$ eV, consistent with the plasmonic band gap of 14 nm given in Ref. [14]. Results for the buildup- and life-times are reported in Table I. Because of spatial integration, the plasmon pulse extension T has little influence on the variance. The values in the table were obtained with $T = 15$ fs (FWHM). A conservative lower bound of T is given by the diameter of the NIR spot size, an upper bound by that size plus plasmon propagation during excitation. Variation in the range of $T = 10$ and 20 fs has only a small effect on buildup and decay times. Due to the superposition of bright mode decay with dark mode buildup, variation is largest for these parameters with about 0.7 fs. For any given value of T in this interval, the buildup and decay extracted from the FDTD surface field and from the spectrogram variance are in good agreement.

A comparison of the two spectrograms in Figure 3 of the NIR vs. the plasmonic field allows the evaluation of the field enhancement, which is in the present case ~ 1. ¿From the spectrogram at grazing direction, we get a NIR pulse duration of $\Delta t_{\mathrm{fwhm}} = 4.5$ fs, in good agreement with the 4.6 fs from the FDTD code. Such a measurement provides an independent *in situ* diagnosis of the field distortions of the NIR field caused by the interaction with the grating.

In conclusion, we have shown how to obtain, with existing experimental instrumentation, direct, time-resolved images of the SPP surface field. Time resolution is determined by controlling the relative pulse delay. This allows the extraction of basic parameters such as SPP buildup and life times. Attosecond resolution, in our example, provides for the distinction of bright and dark mode oscillations. The same setup also provides *in situ* diagnostics of the NIR pulse.

Once spatially separated XUV attosecond and NIR pulses become available, one may resolve in space and time also other surface phenomena: by letting the NIR field excite a surface mode in some region, one can image SPP propagation along complex plasmonic waveguides or plasmonic switches by simply pointing the attosecond XUV pulse on the region of interest.

We are grateful to C. Ropers for useful discussions. We acknowledge support by the DFG, by the excellence cluster "Munich Center for Advanced Photonics (MAP)", by the Austrian Science Foundation project ViCoM (F41), by the Landesexzellenzcluster "Frontiers in Quantum Photon Science" and the Joachim Herz Stiftung.

* mattia.lupetti@physik.uni-muenchen.de; armin.scrinzi@lmu.de

[1] E. Ozbay, Science **311**, 189 (2006).
[2] C. Ropers, D. Park, G. Stibenz, G. Steinmeyer, J. Kim, D. Kim, and C. Lienau, Physical review letters **94**, 113901 (2005).
[3] R. Kienberger, E. Goulielmakis, M. Uiberacker, A. Baltuska, V. Yakovlev, F. Bammer, A. Scrinzi, T. Westerwalbesloh, U. Kleineberg, U. Heinzmann, M. Drescher, and F. Krausz, Nature **427**, 817 (2004).
[4] A. L. Cavalieri, N. Müller, T. Uphues, V. S. Yakovlev, A. Baltuska, B. Horvath, B. Schmidt, L. Blümel, R. Holzwarth, S. Hendel, M. Drescher, U. Kleineberg, P. M. Echenique, R. Kienberger, F. Krausz, and U. Heinzmann, Nature **449**, 1029 (2007).
[5] M. Hentschel, R. Kienberger, C. Spielmann, G. A. Reider, N. Milosevic, T. Brabec, P. Corkum, U. Heinzmann, M. Drescher, and F. Krausz, Nature **414**, 509 (2001).
[6] P. Corkum, Phys. Rev. Lett. **71**, 1994 (1993).
[7] P. Agostini and L. F. DiMauro, Reports Prog. Phys. **67**, 813 (2004).
[8] W. Barnes, Physical Review B **54**, 6227 (1996).
[9] F. Süßmann and M. F. Kling, Physical Review B **84** (2011).
[10] S. Neppl, R. Ernstorfer, E. M. Bothschafter, A. L. Cavalieri, D. Menzel, J. V. Barth, F. Krausz, R. Kienberger, and P. Feulner, Phys. Rev. Lett. **109**, 087401 (2012).
[11] A. Taflove, *Computational Electrodynamics: The Finite - Difference* (1995).
[12] A. F. Oskooi, D. Roundy, M. Ibanescu, P. Bermel, J. Joannopoulos, and S. G. Johnson, Comput. Phys. Commun. **181**, 687 (2010).
[13] A. D. Rakić, A. B. Djurišić, J. M. Elazar, and M. L. Majewski, Appl. Opt. **37**, 5271 (1998).
[14] C. Ropers, T. Elsaesser, G. Cerullo, M. Zavelani-Rossi, and C. Lienau, New Journal of Physics **9**, 397 (2007).